A nomogram for predicting nutritional risk before surgery for gastric cancer

doi: 10.6133/apjcn.202406/PP.0014
Published online: June 2024

Running title: Nomogram for nutritional risk

Changhua Li PhD[1], Jinlu Liu PhD[1], Congjun Wang PhD[2], Yihuan Luo PhD[3], Lanhui Qin PhD[4], Peiyin Chen PhD[4], Junqiang Chen MD, PhD[1,2,3,4]

[1]Department of Gastrointestinal Surgery, The First Affiliated Hospital of Guangxi Medical University, Nanning, China
[2]Guangxi Key Laboratory of Enhanced Recovery after Surgery for Gastrointestinal Cancer, The First Affiliated Hospital of Guangxi Medical University, Nanning, China
[3]Guangxi Clinical Research Center for Enhanced Recovery after Surgery, The First Affiliated Hospital of Guangxi Medical University, Nanning, China
[4]Guangxi Zhuang Autonomous Region Engineering Research Center for Artificial Intelligence Analysis of Multimodal Tumor Images, The First Affiliated Hospital of Guangxi Medical University, Nanning, China

Authors' email addresses and contributions:
CL: lichanghua@sr.gxmu.edu.cn
Contribution: study design, supervision of data collection, data analysis and interpretation, and writing the manuscript.

JL: liujinlugx@163.com
Contribution: study design, supervision of data collection, data analysis and interpretation, and revised the manuscript.

CW: wangcongjun1201@126.com
Contribution: data software analysis.

YL: 904734947@qq.com
Contribution: data collection.

LQ: mandychum7@outlook.com
Contribution: image feature extraction.

PC: 840885693@qq.com
Contribution: image feature extraction.

Corresponding Author: Prof. Junqiang Chen, Department of Gastrointestinal Surgery, The First Affiliated Hospital of Guangxi Medical University, Nanning, China 530021. Tel: 0771-5356701. Email: chenjunqiang@gxmu.edu.cn

ABSTRACT

Background and Objectives: Gastric cancer (GC) is the fourth leading cause of cancer death worldwide. Patients with GC have higher nutritional risk. To construct a nomogram model for predicting preoperative nutritional risk in patients with GC in order to more precisely assess preoperative nutritional risk in patients. **Methods and Study Design:** Patients diagnosed with GC and undergoing surgical treatment were included in this study. Data was collected through clinical information, laboratory testing, and radiomics-derived characteristics. The use of the least absolute shrinkage selection operator (LASSO) regression analysis and multi-variable logistic regression is employed to construct a clinical prediction model, which takes the form of a logistic nomogram. The effectiveness of the nomogram model was evaluated using receiver operating characteristic (ROC) curve, calibration curve, and decision curve analysis (DCA). **Results:** A total of three predictors, namely body mass index (BMI), hemoglobin (Hb) and radiomics characteristic score (Radscore) were identified by LASSO regression analysis from a total of 18 variables studied. The model constructed using these three predictors displayed medium prediction ability. The area under the ROC curve was 0.895 (95% CI 0.844-0.945) in the training set, with a cutoff value of 0.651, precision of 0.957, and sensitivity of 0.718. In the validation set, it was 0.880 (95% CI 0.806-0.954), with a cutoff value of 0.655, precision of 0.930, and sensitivity of 0.698. DCA also confirmed the clinical benefit of the combined model. **Conclusions:** This simple and dependable nomogram model for clinical prediction can assist physicians in assessing preoperative nutritional risk in GC patients in a time-efficient and accurate manner to facilitate early identification and diagnosis.

Key Words: nutritional risk, nomogram, radiomics, prediction, gastric cancer

INTRODUCTION

Gastric cancer (GC) is a widely widespread malignancy on a global scale, occupying the fifth position in terms of incidence and the fourth position in terms of death. According to the American Cancer Society (2020), it is projected that approximately 769,000 individuals will succumb to this illness.[1] The major therapeutic approach for advanced GC continues to be surgical resection, whereby minimally invasive techniques and surgical robotics have played a significant role in reducing patient trauma. Nevertheless, the long-term prognosis of GC is impacted by perioperative complications induced by nutritional risk.[2-4] GC patients cannot avoid nutrient deficiency, nutrient absorption disorder, cachexia, and other complications caused by tumor consumption. They are prevalent perioperative complications that will

negatively affect the prognosis of patients with GC.[5-7] Individualized nutrition therapy for patients with GC is receiving increasing attention from clinicians, and effective nutrition therapy will enhance clinical outcomes.[8] Detecting the nutritional risk in patients with GC in a timely and accurate manner is an urgently needed clinical solution.

Nutritional Risk Assessment 2002 (NRS2002) is a nutritional risk screening tool widely used clinically. It aims to identify individuals at nutritional risk among hospitalized patients so that intervention measures can be taken at an early stage. Assessing cancer patients' nutritional risks and treating their malnutrition aggressively may increase their quality of life.[9] There is a close relationship between the mass of skeletal muscle and the nutritional status of the human body. Due to malnutrition and protein absorption disorders in patients with GC, the incidence of skeletal muscle mass loss is high, which will have a negative impact on the prognosis of patients.[10,11] Radiomics has the potential to study skeletal muscle mass, and some studies have established the reliability of using psoas characteristics of the third lumbar vertebra (L3) as an indicator of skeletal muscle mass loss.[12-14] Our previous study demonstrated a correlation between the area of the L3 psoas major muscle and the nutritional risk,[12] further deep learning for radiomics image processing and quantification may aid in thoroughly evaluating cancer patients' preoperative nutritional status.

The potential for subjective misunderstandings among the participants and the limited scope of the questionnaire's one-way communication may compromise the reliability of the rating results. As a result, we performed a study at a single medical facility to analyse clinical data from individuals diagnosed with advanced GC. The objective of this study is to identify and validate the factors that influence the preoperative nutritional risk of individuals diagnosed with GC. Additionally, the study aims to develop a reliable risk model that can accurately predict the preoperative nutritional risk in patients with advanced GC. The ultimate goal is to enhance the detection rate of nutritional risk in GC patients and establish a well-founded nutritional pre-rehabilitation program that encompasses comprehensive evaluation and effective management of perioperative nutritional status.

MATERIALS AND METHODS

Patients

A retroactive study was conducted on a cohort of 343 patients who were diagnosed with GC and had surgical treatment at the Department of Gastrointestinal Surgery at the First Affiliated Hospital of Guangxi Medical University during the period from January 2016 to December 2019. Patients met the following inclusion criteria in this study: (1) a histological

confirmation of primary GC, (2) comprehensive clinical data including laboratory test results obtained within two weeks period prior to surgery, and (3) the absence of any significant organ malfunction. The exclusion criteria encompassed three factors: (1) inadequate data, (2) coexistence of other malignant tumors, and (3) substandard picture quality or discernible distortions surrounding the L3 psoas muscle.

This study was performed in accordance with the guidelines outlined in the Declaration of Helsinki and was approved by the Ethics Committee of the First Affiliated Hospital of Guangxi Medical University. Since the study was a retrospective study, most of the study subjects have died or lost contacts, and all statistics were anonymous, so the Ethics Committee of the First Affiliated Hospital of Guangxi Medical University agreed to waive the need for informed consent.

Nutritional assessment

The nutritional risk in GC patients undergoing surgery was evaluated using the Chinese version of NRS2002 by a trained nutritional support team in the hospital ward. NRS2002 assessment tool has two distinct components. The first section of the analysis assesses the nutritional condition of the patient and addresses any recent challenges encountered in food consumption. Subsequently, the subsequent section presents data about the influence of illness severity on the individual's nutritional status. Each section is scored on a scale of 0-3, with additional points given to patients aged $\geq$ 70 years. The NRS2002 total score ranges from 0-7. An NRS2002 score of $\geq$ 3 indicates a nutritional risk, while a score of < 3 indicates no immediate nutritional risk.

Data collection

The computerized case system utilized by the First Affiliated Hospital of Guangxi Medical University is responsible for the collection of demographic and clinical information. This includes data pertaining to age, gender, height, weight, smoking history, family history and tumor TNM staging. Blood samples were collected in order to assess a range of laboratory parameters, which encompassed hemoglobin (Hb), white blood cell count (WBC), neutrophil count (NEUT), total lymphocyte count (TLC), albumin (ALB), prealbumin (PAB), total cholesterol (TC), carcinoembryonic antigen (CEA), alpha-fetoprotein (AFP), tumor marker CA199, tumor marker CA125, and tumor marker CA153. The laboratory measures of peripheral venous blood were performed within two weeks timeframe preceding the surgical

procedure. BMI)was determined by dividing the respondent's kilogram weight by their square meter height.

Texture feature extraction and selection

Participants in this study had computed tomography (CT) scans of their abdomens before receiving surgical procedure. The picture segmentation process involved utilizing the 3D-Slicer software, specifically version 4.10.2, which is considered stable. The objective was to outline the left and right L3 psoas muscles as the designated volume of interest (Supplementary Figure 2). To mitigate any interference from neighboring fat, bone, and surrounding organs, pixels exhibiting attenuation values below -50 HU or above 100 HU were eliminated from the analysis. The intra-observer ICC, as determined by two reader one extractions, varied between 0.853 and 0.928. Between two readers (L.Q. and P.C.), the inter-observer agreement ranged from 0.846 to 0.907. The results showed good intra- and inter-observer feature extraction agreements.

The Pyradiomics (v3.6.2) software package was utilized to extract radiomics features. First-order statistical features (IH, intensity histogram), shape-based histogram features, and texture features were extracted from the volume of interest (VOI). The image underwent preprocessing using wavelet filtering, followed by the extraction of texture features from the pre-processed image. Using Haar wavelet as filter, three-layer wavelet decomposition is set up to effectively remove noise while preserving image details. In threshold processing, the soft threshold method is selected, which is automatically adjusted according to the coefficient distribution after each layer decomposition to achieve the best noise reduction effect. The Z-Score method normalizes image by subtracting (μmuscle), corresponding to the mean intensity value of the considered ROI (here, the muscle) in training set, from each voxel intensity I(x) and dividing the result by the standard deviation of the ROI (σmuscle).[17] The same mean and standard deviation were applied to normalize the validation set data:

$$I_{z\text{-}score}(x) = [I(x) - \mu_{muscle}] / \sigma_{muscle}$$

The data were further processed to reduce dimension, Spearman's correlation coefficient was first used to remove features with a correlation coefficient greater than 0.9. Then, using the R glmnet software package, the minimum absolute contraction and selection operator (LASSO) was run to reduce the dimensionality of the features again, and the radiomic features related to nutritional risk diagnosis were screened. The calculation of a radiomics signature score (referred to as Radscore) was performed for each patient by applying coefficients that were weighted using the LASSO logistic regression model in the training set.

For each volume of interest (VOI), a comprehensive set of 102 raw characteristics and 558 wavelet features were gathered (shown in Table S1). Within the dataset, there exist a total of 102 distinct features. There are 18 first-order statistical features, 9 histogram features based on shape, 24 Gray Level Co-occurrence Matrix (GLCM) features, 14 Gray Level Dependence Matrix (GLDM) features, 16 Gray Level Run Length Matrix (GLRLM) features, 16 Gray Level Size Zone Matrix (GLSZM) features, and 5 Neighboring Gray Tone Difference Matrix (NGTDM) features. The radiomic features mentioned in this context have been previously defined in mathematical terms.[15] These definitions can be accessed at the following URL: https://pyradiomics.readthedocs.io/en/latest/.

Statistical analysis

The statistical analysis was done in R, version 4.2.0, developed by the R Foundation for Statistical Computing in Vienna, Austria. Using the R caret package, the GC patients were randomly split into a training set and a validation set, following a 7:3 ratio. Descriptive statistics were used to summarize the baseline characteristics. Continuous data were reported in the form of medians and interquartile ranges, while categorical information was presented in the form of percentages. Statistical methods, including Pearson's chi-square test, Fisher's exact test, Mann-Whitney test, and McNemar's test, were used to conduct group comparisons for both categorical and continuous data, as deemed suitable for this study. The selection and adjustment of predictors were performed using LASSO regression analysis.[16]

A prediction model for assessing the nutritional risk was constructed through the utilization of logistic regression analysis. This was achieved by amalgamating specific features within the LASSO regression model. To obtain the subset of predictors, the LASSO regression analysis minimizes prediction error for a quantitative response variable by imposing a constraint on the model parameters that cause the regression coefficients for some variables to shrink toward zero. Use the glmnet package to run LASSO, because the included dependent variable is whether the NRS2002 score is <3 or ≥3, based on type measures of -2loglikelihood and binomial family, the LASSO regression analysis run in R software runs 10x cross-validation to centralize and standardize the included variables, and then select the best lambda value. 1SE gives a model with good performance but minimal number of independent variables. So the LASSO method was used to analyse the data in the training set to select the optimal predictors of the present risk factors. A nomogram was built based on the concept proposed in reference.18 The qualities that were reported are presented in the form of odds ratios (OR) along with corresponding 95% confidence intervals (CI). In this study, Statistical

significance was assessed by evaluating two-tailed p-values that were below the threshold of 0.05. The Receiver Operating Characteristic (ROC) software was used to distinguish between genuine positives and false positives in the nutritional risk nomogram.[19] At the same time, the confusion matrix (R caret package) is used to evaluate the model performance. The nutrition risk nomogram's calibration was evaluated using calibration curves, and its clinical appropriateness was assessed using decision curve analysis (DCA) by analysing the net benefit at different threshold probabilities (Figure 1).

RESULTS

Patient baseline data

This study included a cohort of 284 patients diagnosed with GC, with 181 males and 103 females. The GC patients were allocated randomly to either the training set (n=198) or the validation set (n=86). The baseline characteristics of the two groups of patients are shown in Table 1.

At baseline, age, gender, BMI, T stage, N stage, hemoglobin (Hb), albumin (ALB), prealbumin (PAB), neutrophil count (NEUT), total lymphocyte count (TLC), total cholesterol (TC), carcinoembryonic antigen (CEA), alpha-fetoprotein (AFP), tumor markers (CA125, CA153, CA199) and Radscore were assessed. There were no statistically significant differences seen in these characteristics between the two groups (p>0.05), indicating comparability. Inter-group analysis of study variables stratified by NRS2002 status (positive and negative) is shown in the Supplementary Table 3.

Radscore building based on radiomics features

The dimension of the extracted radiomics features was reduced using LASSO logistic regression (Figure S1), and the significant features were identified in the training set. A total of six radiomics features were screened out (Table S2). The Radscore was calculated as follows:0.4545577175631209+0.04341*gradient_glcm_Imc2+0.01522*gradient_glrlm_LowGrayLevelRunEmphasis+0.03121*gradient_glszm_SmallAreaLowGrayLevelEmphasis+0.024431*gradient_ngtdm_Coarseness+0.019694*waveletLH_gldm_SmallDependenceLowGrayLevelEmphasis+0.005178*wave-let-LL_glszm_SmallAreaLowGrayLevelEmphasis.

Independent risk factors in the training set

This study included a total of eighteen factors pertaining to clinical symptoms, laboratory testing and radiological score. The coefficient distribution plots were created using the log(λ)

sequence. By plotting the partial probability deviation (binomial deviation) versus log(lambda), we were able to determine the optimal parameter (lambda) in the LASSO model, and then we used the one standard error (1SE) criterion Wire to emphasize the vertical line with dots. By using lambda 1SE, we identified three variables with non-zero coefficients (Figure 2).

Predictive model construction

The LASSO regression analysis was used to select three predictive variables, which were further analysed using both univariate and multivariate logistic regression analyses (Table 2). Three predictive factors, BMI, Hb and RadScore constructed from radiomics features, were identified with statistically significant differences. A predictive model was developed using multivariate logistic regression, incorporating these variables, to create a preoperative nutritional risk nomogram for GC (Figure 3).

Predictive model validation

Receiver operating characteristic (ROC) curves and confusion matrix were used to assess the sensitivity and specificity of the prediction models. The performance of the predictive models was assessed using a training set, yielding an area under the curve (AUC) value of 0.895 (95% CI 0.844-0.945), a cutoff value of 0.651, a precision of 0.957, and a sensitivity of 0.718. Similarly, the models were tested using a validation set, resulting in an AUC of 0.880 (95% CI 0.806-0.954), a cutoff value of 0.655, a precision of 0.930, and a sensitivity of 0.698. The combined nomograms AUC and confusion matrix demonstrated fair to good performance (Figure 4). We also compared the combined model with the clinical model and the radiomics model (Supplementary Figure 3).

The prediction models were calibrated using calibration curves and the Hosmer-Lemeshow test, and the p-value of the Hosmer-Lemeshow test for the training set is 0.689, and the p-value of the Hosmer-Lemeshow test for the validation set is 0.7346. The calibration curve reveals strong alignment between the projected model and validation set. The Hosmer-Lemeshow study shows remarkable agreement between calculated and observed probabilities (Figure 5). The nomogram DCA also suggests that this model could be valuable in a clinical setting (Figure 6).

DISCUSSION

Malnutrition is a significant clinical issue in patients with GC, which can impact both treatment effectiveness and patients' quality of life. The initial step in preventing and treating malnutrition in these patients is to conduct nutritional risk screening. It is crucial to promptly and accurately identify the nutritional risk, followed by a comprehensive nutritional assessment to diagnose malnutrition. This allows clinicians to take appropriate measures for GC patients. Adequate nutritional interventions and support can enhance the patient's treatment response and expedite their recovery. In this study, we retrospectively analysed relevant data of GC patients before surgical treatment to develop and validate a nomogram model. This model combines clinical data and radiological features (Radscore) to predict nutritional risk in GC patients before surgical treatment. By utilizing this model, clinicians can make informed clinical decisions and implement a comprehensive assessment and diagnosis of nutritional risk in GC patients before surgical treatment.

NRS2002 is a well-known method for detecting individuals at nutritional risk, and it is often used for nutritional screening in cancer patients. According to research by Zang et al., cancer patients at risk of malnutrition had a reduced overall survival rate and an increased likelihood of developing complications after surgery.[20] However, a multicenter study utilized NRS2002 to evaluate the nutritional risk among individuals with gastrointestinal diseases. The findings revealed that the prevalence of malnutrition among individuals diagnosed with gastrointestinal cancer was a mere 17.6%, certain patients diagnosed with GC evaded detection by screening instruments.[21] Furthermore, a comparative analysis of the diagnostic accuracy of various nutrition screening instruments for adult malnutrition was conducted by Cheung et al. NRS2002 demonstrated exceptional diagnostic capability but a 27.7% rate of missed diagnoses.[22] False negative results of nutritional risk screening may be more detrimental to cancer patients than false positive results. The improvement of cancer nutritional risk assessment is a clinical issue that requires resolution. We were motivated by the study of Xie et al., who coupled systemic inflammatory indicators with GLIM criteria and found that GLIM criteria based on inflammatory markers had greater predictive power in assessing the short-term and long-term prognosis of cancer patients.[23] Consequently, we maintain the conviction that the multi-dimensional nutritional risk prediction system for patients diagnosed with GC has practical applicability in the clinic, in an effort to construct a predictive model that incorporates radiomics features and clinical data. It has been validated that the model possesses decent predictive ability. (AUC > 0.8).

Hemoglobin levels may be used to indicate the nutritional risk in patients. Hb declines as malnutrition progresses, and investigations have verified this association.[24,25] However, Zhou et al. discovered that only the Hb index was employed to evaluate the nutritional status of hospitalized patients, and the percentage of nutritional risk identification was only 24%.[26] Similarly, BMI is an indicator that is used to analyse the connection between weight and height, giving information on a person's weight status and reflecting some nutritional status features.[27,28] Although the NRS2002 includes BMI as an auxiliary indication for nutritional risk screening, assessing nutritional status just by utilizing the scale's BMI cut-off points may be inaccurate. Several tools were employed in a study to evaluate the nutritional health condition of elderly inpatients. The findings revealed that the detection rate of risk screening based just on BMI was the lowest, at 23.7%.[29] As a result, assessing patients' nutritional status only on a single indicator is insufficient. Our findings show that BMI and Hb are independent risk factors for preoperative nutritional risk in patients with GC. This prediction model may thoroughly analyse patients' nutritional status using numerous criteria, optimize the importance of risk factors, and increase the accuracy of preoperative nutritional risk screening.

Radiomics is an emerging image analysis method that can convert CT, MRI, and PET-CT images into high-throughput radiomics feature data.[30] These features can then be used to establish radiomics by linear or nonlinear machine learning methods, which can be further analyzed.[31] Studies have reported that radiomics features can be used to predict sarcopenia in patients with GC, and that it is associated with the prognosis of these patients. For example, Lan et al. used CT images to extract radiomics features of sarcopenia and combined them with a clinical prediction model to individually predict postoperative complications in patients with GC, showing good prediction performance (training set AUC is 0.763).[32] Chen et al. used LASSO analysis to identify 14 psoas major muscle radiomics features, which were then incorporated in the radiomics scoring model. The subjectivity of sarcopenia assessment was minimized after quantitative examination, and prediction accuracy was enhanced.[33] The methodologies outlined above are utilized in this study, radiomics data from the psoas major muscle at the L3 level were retrieved from CT images of 284 individuals with GC. Six relevant radiomics features were chosen for the scoring model and then coupled with clinical data to create a nomogram model to predict the preoperative nutritional risk in patients. In these radiomics features, Gray-level co-occurrence matrix (GLCM) represents second-order statistics, which describe the correlation of neighboring voxels according to different angles. Gray-level run length matrix (GLRLM) represents run length of similar gray-level in the

image. Gray-level size zone matrix (GLSZM) represents different gray-level zones in the image and their distribution. Neighboring gray tone difference matrix (NGTDM) represents the difference between gray-level and the average within certain distances. Gray-level-dependent matrix (GLDM) represents gray-level dependencies independent from angles.[34,35] In consideration of physical condition and radiomics score, the model is capable of conducting a comprehensive evaluation of patients' nutritional status. The nomogram presents clinically relevant recommendations for comprehensive screening of nutritional risk by displaying the proportion of each influential factor.

This study focuses on the integration of clinical data and imaging studies, which are crucial components in the development of a clinical practice prediction system. Our established clinical prediction model is user-friendly and enables accurate and prompt assessment of nutritional risk in GC patients. It has undergone comprehensive and successful verification. However, our clinical prediction model does have certain limitations. Firstly, the sample size of this study is modest, and it is required to raise the sample size in the future in order to enhance the correlation of radiomics scores and to collaborate with other institutions for external verification. Secondly, in future clinical studies, the model can be further improved by incorporating body composition analysis to better cater to the needs of gastrointestinal surgeons. Furthermore, apart from NRS2002, there are several other excellent nutrition assessment tools that are widely used in clinical settings. The integration of multiple screening tools may offer valuable insights into the clinical potential of the nutritional risk nomogram prediction model.

Conclusion

Based on the laboratory examination, pathological data and analysis of clinical data and radiomics features of GC patients conducted at our institution, we found that BMI, Hb and Radscore were independent risk factors for preoperative nutritional risk in GC patients. To assist doctors in assessing the nutritional risk in GC patients before surgical treatment, we have developed a simple and repeatable nomogram clinical prediction model. This model can effectively guide doctors in identifying and diagnosing GC patients at nutritional risk.

ACKNOWLEDGEMENTS

Thanks for the support of Lifeng Tao, Bo Shi, and Meile Mo.

CONFLICT OF INTEREST AND FUNDING DISCLOSURE

The authors declare no conflict of interest.

This research was funded by the National Natural Science Foundation of China [grant no.82060430], Guangxi Clinical Research Center for Enhanced Recovery after Surgery; Guangxi Science and Technology Base and Talent Project [grant no.AD19245196], the Guangxi Key Research and Development Project [grant no. AB18126058], Guangxi key Laboratory of Enhanced Recovery after Surgery for Gastrointestinal Cancer [grant no. YYZS2020003].

REFERENCES

1. Sung H, Ferlay J, Siegel RL, Laversanne M, Soerjomataram I, Jemal A, et al. Global Cancer Statistics 2020: GLOBOCAN Estimates of Incidence and Mortality Worldwide for 36 Cancers in 185 Countries. CA Cancer J Clin. 2021; 71: 209-249. doi: 10.3322/caac.21660.
2. Solaini L, Bazzocchi F, Pellegrini S, Avanzolini A, Perenze B, Curti R, Morgagni P, Ercolani G. Robotic vs open gastrectomy for gastric cancer: A propensity score‐matched analysis on short‐and long‐term outcomes. The International Journal of Medical Robotics and Computer Assisted Surgery. 2019; 15:e2019. doi: 10.1002/rcs.2019.
3. Puértolas N, Osorio J, Jericó C, Miranda C, Santamaría M, Artigau E, et al. Effect of Perioperative Blood Transfusions and Infectious Complications on Inflammatory Activation and Long-Term Survival Following Gastric Cancer Resection. Cancers. 2022; 15:144.doi: 10.3390/cancers15010144.
4. Yuan P, Wu Z, Li Z, Bu Z, Wu A, Wu X, Zhang L, Shi J, Ji J. Impact of postoperative major complications on long-term survival after radical resection of gastric cancer. BMC Cancer. 2019; 19:833. doi: 10.1186/s12885-019-6024-3.
5. Fukuda Y, Yamamoto K, Hirao M, Nishikawa K, Maeda S, Haraguchi N, et al. Prevalence of Malnutrition Among Gastric Cancer Patients Undergoing Gastrectomy and Optimal Preoperative Nutritional Support for Preventing Surgical Site Infections. Annals of Surgical Oncology. 2015; 22: 778-785. doi: 10.1245/s10434-015-4820-9.
6. Fujiya K, Kawamura T, Omae K, Makuuchi R, Irino T, Tokunaga M, Tanizawa Y, Bando E, Terashima M. Impact of Malnutrition After Gastrectomy for Gastric Cancer on Long-Term Survival. Annals of Surgical Oncology. 2018; 25: 974-983. doi: 10.1245/s10434-018-6342-8.
7. GlobalSurg Collaborative and NIHR Global Health Unit on Global Surgery. Impact of malnutrition on early outcomes after cancer surgery: an international, multicentre, prospective cohort study. Lancet Glob Health. 2023; 11: e341-e349. doi: 10.1016/s2214-109x(22)00550-2.
8. Sakurai K, Ohira M, Tamura T, Toyokawa T, Amano R, Kubo N, et al. Predictive Potential of Preoperative Nutritional Status in Long-Term Outcome Projections for Patients with Gastric Cancer. Annals of Surgical Oncology. 2015; 23: 525-533. doi: 10.1245/s10434-015-4814-7.

9. Cao J, Xu H, Li W, Guo Z, Lin Y, Shi Y, et al. Nutritional assessment and risk factors associated to malnutrition in patients with esophageal cancer. Current Problems in Cancer. 2021; 45:100638. doi: 10.1016/j.currproblcancer.2020.100638.
10. Matsui R, Inaki N, Tsuji T. Impact of visceral adipose tissue on long-term outcomes after gastrectomy for advanced gastric cancer. Nutrition. 2022; 97: 111619. doi: 10.1016/j.nut.2022.111619.
11. Zhao A, Hou C, Li Y, Liu Y. Preoperative low muscle mass and malnutrition affect the clinical prognosis of locally advanced gastric cancer patients undergoing radical surgery. Frontiers in Oncology. 2023; 13:1156359. doi: 10.3389/fonc.2023.1156359.
12. Shi B, Liu S, Chen J, Liu J, Luo Y, Long L, Lan Q, Zhang Y. Sarcopenia is Associated with Perioperative Outcomes in Gastric Cancer Patients Undergoing Gastrectomy. Annals of Nutrition and Metabolism. 2019; 75: 213-222. doi: 10.1159/000504283.
13. Trestini I, Sperduti I, Sposito M, Kadrija D, Drudi A, Avancini A, et al. Evaluation of nutritional status in non-small-cell lung cancer: screening, assessment and correlation with treatment outcome. ESMO Open. 2020; 5:e000689. doi: 10.1136/esmoopen-2020-000689.
14. Wang WF, Lin CW, Xie CN, Liu HT, Zhu MY, Huang KL, Teng HL. The association between sarcopenia and osteoporotic vertebral compression refractures. Osteoporosis International. 2019; 30: 2459-2467. doi: 10.1007/s00198-019-05144-x.
15. van Griethuysen JJM, Fedorov A, Parmar C, Hosny A, Aucoin N, Narayan V, Beets-Tan RGH, Fillion-Robin JC, Pieper S, Aerts HJWL. Computational Radiomics System to Decode the Radiographic Phenotype. Cancer Research. 2017; 77: e104-e107. doi: 10.1158/0008-5472.Can-17-0339.
16. Liu J, Huang J, Ma S, Wang K. Incorporating group correlations in genome-wide association studies using smoothed group Lasso. Biostatistics. 2013; 14: 205-219. doi: 10.1093/biostatistics/kxs034.
17. Cheadle C, Vawter MP, Freed WJ, Becker KG. Analysis of microarray data using Z score transformation. J Mol Diagn. 2003; 5: 73-81. doi: 10.1016/s1525-1578(10)60455-2.
18. Wang H, Zhang L, Liu Z, Wang X, Geng S, Li J, Li T, Ye S. Predicting medication nonadherence risk in a Chinese inflammatory rheumatic disease population: development and assessment of a new predictive nomogram. Patient Preference and Adherence. 2018;12:1757-1765. doi: 10.2147/ppa.S159293.
19. Lätti S, Niinivehmas S, Pentikäinen OT. Rocker: Open source, easy-to-use tool for AUC and enrichment calculations and ROC visualization. Journal of Cheminformatics. 2016; 8:45. doi: 10.1186/s13321-016-0158-y.
20. Zang Y, Xu W, Qiu Y, Gong D, Fan Y. Association between Risk of Malnutrition Defined by the Nutritional Risk Screening 2002 and Postoperative Complications and Overall Survival in Patients with Cancer: A Meta-Analysis. Nutr Cancer. 2023; 75: 1600-1609. doi: 10.1080/01635581.2023.2227402.
21. Rizzi M, Mazzuoli S, Regano N, Inguaggiato R, Bianco M, Leandro G, et al. Undernutrition, risk of malnutrition and obesity in gastroenterological patients: A multicenter study. World Journal of Gastrointestinal Oncology. 2016; 8:563-72. doi: 10.4251/wjgo.v8.i7.563.

22. Cheung HHT, Joynt GM, Lee A. Diagnostic test accuracy of preoperative nutritional screening tools in adults for malnutrition: a systematic review and network meta-analysis. Int J Surg. 2024; 110: 1090-1098. doi: 10.1097/js9.0000000000000845.
23. Xie H, Yuan K, Ruan G, Wei L, Zhang H, Ge Y, et al. Improving the assessment of malnutrition in cancer: Using systemic inflammation markers as a supplement to the inflammation items of the GLIM criteria. Clin Nutr. 2023; 42: 2036-2044. doi: 10.1016/j.clnu.2023.08.020.
24. Konturek PC, Herrmann HJ, Schink K, Neurath MF, Zopf Y. Malnutrition in Hospitals: It Was, Is Now, and Must Not Remain a Problem! Med Sci Monit. 2015; 21: 2969-2975. doi: 10.12659/msm.894238.
25. Weng CH, Hsu CW, Hu CC, Yen TH, Huang WH. Association Between Hemodiafiltration and Hypoalbuminemia in Middle-Age Hemodialysis Patients. Medicine (Baltimore). 2016; 95: e3334. doi: 10.1097/md.0000000000003334.
26. Zhou J, Wang M, Wang H, Chi Q. Comparison of two nutrition assessment tools in surgical elderly inpatients in Northern China. Nutr J. 2015; 14: 68. doi: 10.1186/s12937-015-0054-8.
27. Zhang Z, Pereira S, Luo M, Matheson E. Evaluation of Blood Biomarkers Associated with Risk of Malnutrition in Older Adults: A Systematic Review and Meta-Analysis. Nutrients. 2017; 9:829. doi: 10.3390/nu9080829.
28. Park JH, Kim E, Seol EM, Kong SH, Park DJ, Yang HK, et al. Prediction Model for Screening Patients at Risk of Malnutrition After Gastric Cancer Surgery. Ann Surg Oncol. 2021; 28: 4471-4481. doi: 10.1245/s10434-020-09559-3.
29. Miao JP, Quan XQ, Zhang CT, Zhu H, Ye M, Shen LY, et al. Comparison of two malnutrition risk screening tools with nutritional biochemical parameters, BMI and length of stay in Chinese geriatric inpatients: a multicenter, cross-sectional study. BMJ Open. 2019; 9: e022993. doi: 10.1136/bmjopen-2018-022993.
30. Lambin P, Rios-Velazquez E, Leijenaar R, Carvalho S, van Stiphout RGPM, Granton P, et al. Radiomics: Extracting more information from medical images using advanced feature analysis. European Journal of Cancer. 2012; 48: 441-446. doi: 10.1016/j.ejca.2011.11.036.
31. Gillies RJ, Kinahan PE, Hricak H. Radiomics: Images Are More than Pictures, They Are Data. Radiology. 2016; 278: 563-577. doi: 10.1148/radiol.2015151169.
32. Lan Q, Guan X, Lu S, Yuan W, Jiang Z, Lin H, Long L. Radiomics in Addition to Computed Tomography-Based Body Composition Nomogram May Improve the Prediction of Postoperative Complications in Gastric Cancer Patients. Annals of Nutrition and Metabolism. 2022; 78: 316-327. doi: 10.1159/000526787.
33. Chen XD, Chen WJ, Huang ZX, Xu LB, Zhang HH, Shi MM, Cai YQ, Zhang WT, Li ZS, Shen X. Establish a New Diagnosis of Sarcopenia Based on Extracted Radiomic Features to Predict Prognosis of Patients With Gastric Cancer. Frontiers in Nutrition. 2022; 9:850929. doi: 10.3389/fnut.2022.850929.

34. Zwanenburg A, Vallières M, Abdalah MA, Aerts H, Andrearczyk V, Apte A, et al. The Image Biomarker Standardization Initiative: Standardized Quantitative Radiomics for High-Throughput Image-based Phenotyping. Radiology. 2020; 295: 328-338. doi: 10.1148/radiol.2020191145.
35. Moawad AW, Ahmed A, Fuentes DT, Hazle JD, Habra MA, Elsayes KM. Machine learning-based texture analysis for differentiation of radiologically indeterminate small adrenal tumors on adrenal protocol CT scans. Abdom Radiol (NY). 2021; 46: 4853-4863. doi: 10.1007/s00261-021-03136-2.

Table 1. Characteristics of the 284 patients with gastric cancer involved in the study according to presence/absence of nutritional risk and randomization to training set and validation set

	All patients N=284	Training set N=198	Validation set N=86	p-value
Gender, n (%)				0.208
Male	181 (63.73%)	60 (69.77%)	121 (61.11%)	
Female	103 (36.27%)	26 (30.23%)	77 (38.89%)	
Age(years)	56.00 [46.00;63.25]	55.00 [47.00;63.75]	57.00 [46.00;63.00]	0.978
BMI (kg/m^2)	19.46 [17.74;21.51]	19.32 [17.61;22.18]	19.48 [17.91;21.02]	0.738
NRS2002				0.463
<3	153 (53.87%)	110 (55.56%)	43 (50.00%)	
≥3	131 (46.13%)	88 (44.44%)	43 (50.00%)	
Diabetic, n (%)				0.758
No	272 (95.77%)	82 (95.35%)	190 (95.96%)	
Yes	12 (4.23%)	4 (4.65%)	8 (4.04%)	
Smoking, n (%)				0.190
No	186 (65.49%)	51 (59.30%)	135 (68.18%)	
Yes	98 (34.51%)	35 (40.70%)	63 (31.82%)	
Hb(g/L)	115.90 [99.45;131.05]	114.45 [100.03;128.32]	116.75 [98.40;131.28]	0.492
NEUT(109/L)	3.54 [2.70;4.22]	3.38 [2.75;4.38]	3.56 [2.65;4.19]	0.854
TLC(109/L)	1.75 [1.38;2.21]	1.78 [1.31;2.17]	1.75 [1.41;2.21]	0.774
ALB(g/L)	39.25 [36.70;41.20]	39.30 [36.30;41.10]	39.20 [36.90;41.27]	0.756
PAB(g/L)	212.55 [180.40;256.82]	204.40 [175.00;257.40]	216.35 [182.40;256.32]	0.152
TC(mmol/L)	4.62 [4.05;5.14]	4.58 [3.98;5.01]	4.68 [4.07;5.18]	0.394
AFP(ng/mL)	7.87 [5.58;11.60]	7.35 [5.27;10.85]	8.16 [5.63;11.80]	0.221
CEA(ng/mL)	2.51 [1.85;3.52]	2.50 [1.94;3.46]	2.51 [1.84;3.53]	0.896
CA125(U/mL)	10.55 [7.58;14.64]	11.10 [7.60;16.04]	10.30 [7.56;14.20]	0.770
CA153(U/mL)	7.87 [5.58;11.60]	7.35 [5.27;10.85]	8.19 [5.63;11.80]	0.216
CA199(U/mL)	7.68 [4.18;17.31]	7.03 [3.75;19.56]	7.74 [4.35;16.92]	0.992
T stage				0.651
T0	2 (0.70%)	0 (0.00%)	2 (1.01%)	
T1	59 (20.77%)	20 (23.26%)	39 (19.70%)	
T2	44 (15.49%)	12 (13.95%)	32 (16.16%)	
T3	43 (15.14%)	16 (18.60%)	27 (13.64%)	
T4	136 (47.89%)	38 (44.19%)	98 (49.49%)	
N stage				0.396
N0	108 (38.03%)	35 (40.70%)	73 (36.87%)	
N1	40 (14.08%)	14 (16.28%)	26 (13.13%)	
N2	53 (18.66%)	11 (12.79%)	42 (21.21%)	
N3	83 (29.23%)	26 (30.23%)	57 (28.79%)	
Radscore	7.73 [5.82;14.35]	7.86 [5.89;15.07]	7.73 [5.76;13.76]	0.853

NRS2002, nutritional risk screening 2002; BMI, body mass index; Hb, hemoglobin; ALB, albumin; PAB, prealbumin; NEUT, neutrophile count; TLC, total lymphocyte count; CEA, carcinoembryonic antigen; AFP, alpha-fetoprotein..
p<0.05 meant that the difference was statistically significant.

Table 2. Univariate and multivariate logistic regression were used to screen LASSO regression predictors for nutritional risk

Characteristics	Uni-B	Uni-SE	Uni-OR	Uni-CI	Uni-Z	Uni-p	Multi-B	Multi-SE
BMI	-0.308	0.06691	0.735	0.735 (0.640-0.833)	-4.597	< 0.001	-0.398	0.1264
Hb	-0.059	0.00923	0.943	0.943 (0.925-0.959)	-6.368	< 0.001	-0.053	0.01512
Radscore	0.546	0.07638	1.727	1.727 (1.509-2.042)	7.152	< 0.001	0.57	0.09055

Characteristics	Multi-OR	Multi-CI	Multi-Z	Multi-p
BMI	0.672	0.672 (0.510-0.840)	-3.15	0.002
Hb	0.948	0.948 (0.918-0.975)	-3.518	< 0.001
Radscore	1.769	1.769 (1.511-2.165)	6.3	< 0.001

Values were shown as means±SD.

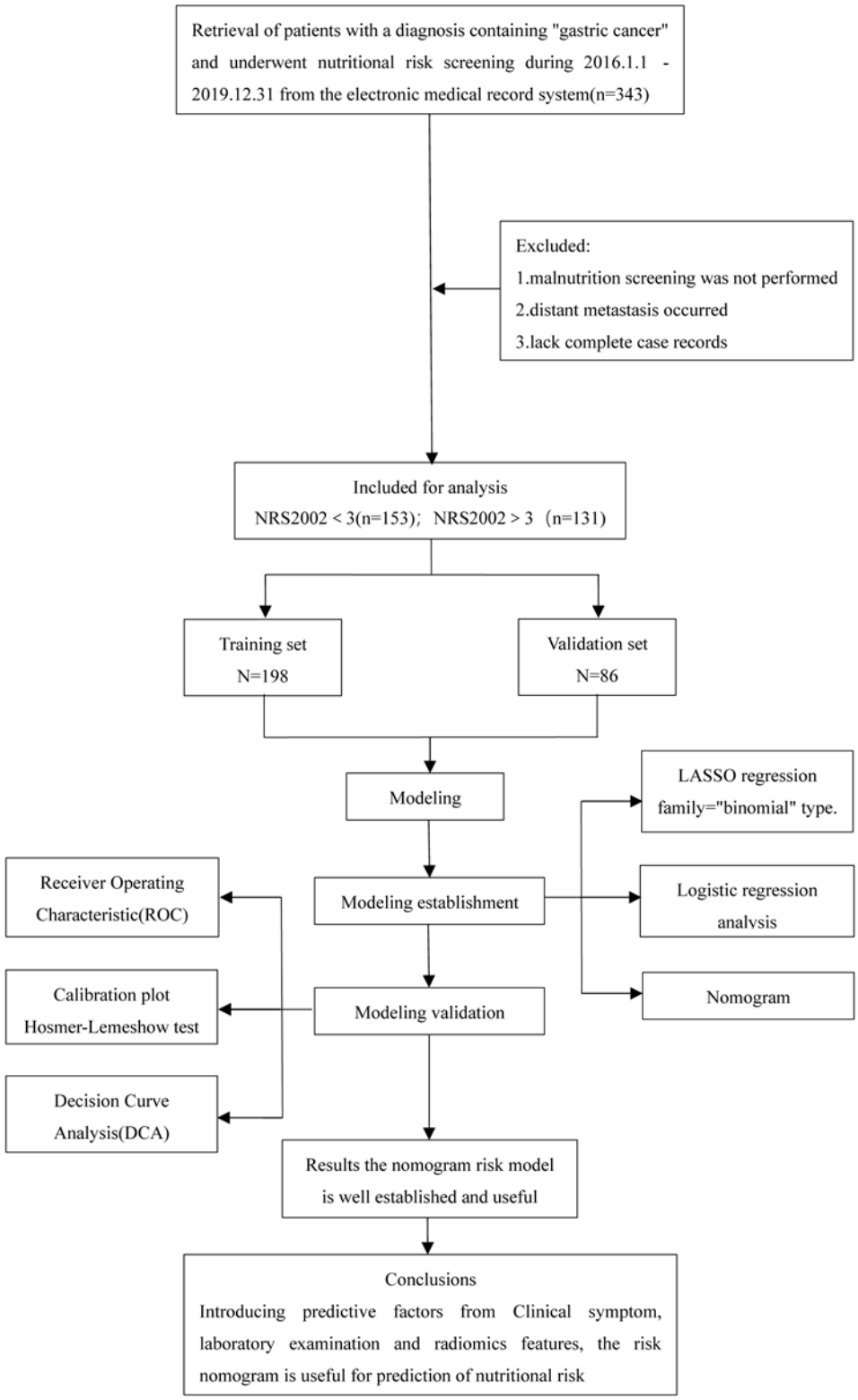

Figure 1. Flow chart of study design. NRS2002, nutritional risk screening 2002; LASSO, least absolute shrinkage and selection operator; ROC, receiver operating characteristic; DCA, decision curve analysis.
$^{\dagger}p<0.05$ compared with Gp1; $^{\ddagger}p<0.05$ compared with Gp2; $^{\S}p<0.05$ compare with Gm1; $^{\P}p<0.05$ compared with Gm2; $^{\dagger\dagger}p<0.05$ compared with Gm3.

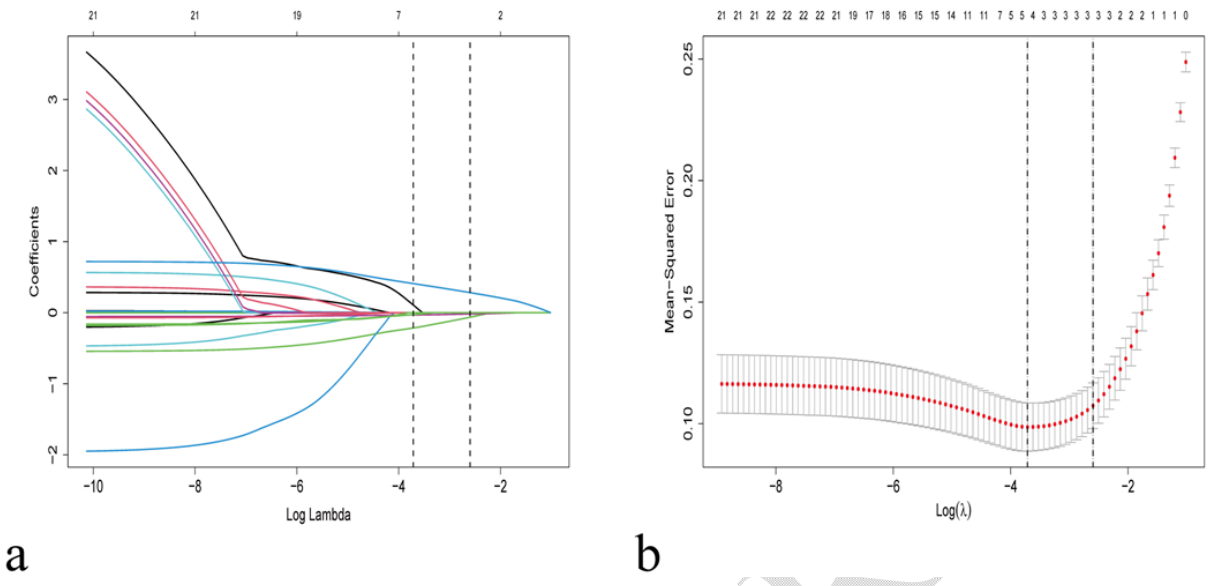

Figure 2. Variable selection using LASSO for binary logistic regression. (a) The optimum lambda selected twenty-one nonzero coefficient variables. Each line represented a parameter with a vertical coefficient at its end. (b) After validating the optimal parameter (lambda) in the LASSO model, the partial likelihood deviance (binomial deviance) curve was plotted against log (lambda) and vertical dashed lines were constructed based on 1 standard error threshold.

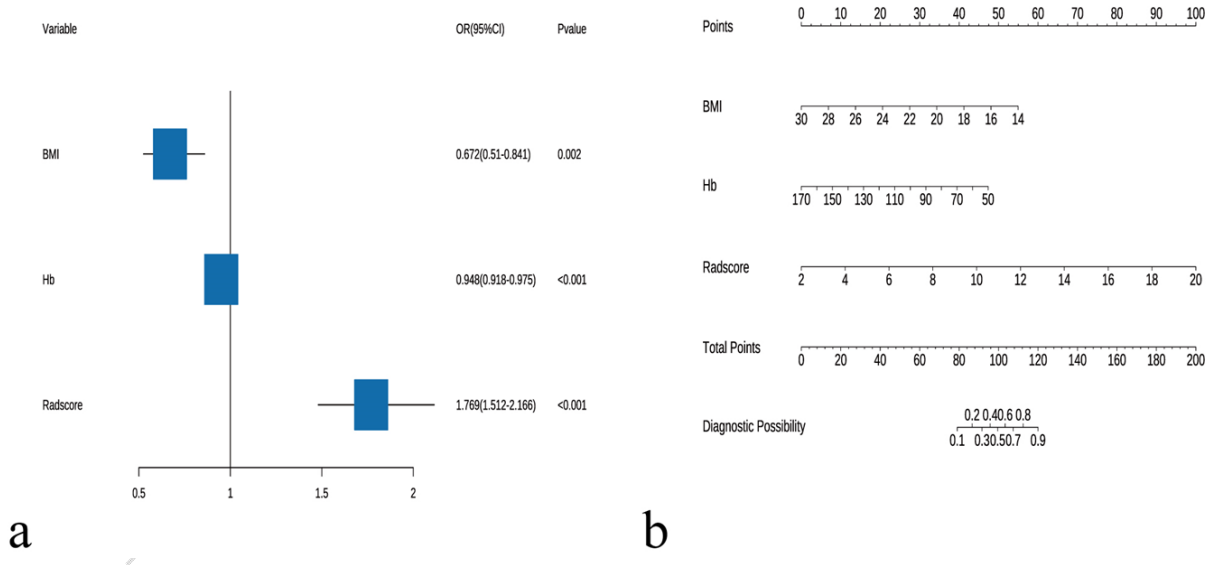

Figure 3. Multivariate logistic regression created the prediction model. (a) Multivariate logistic regression analysis of nutritional risk predictors. (b) Nomogram for nutritional risk prediction in gastric cancer patients. OR, CI, and p values are all shown. p<0.05 indicated a statistically significant difference. OR, odds ratio; CI, confidence interval

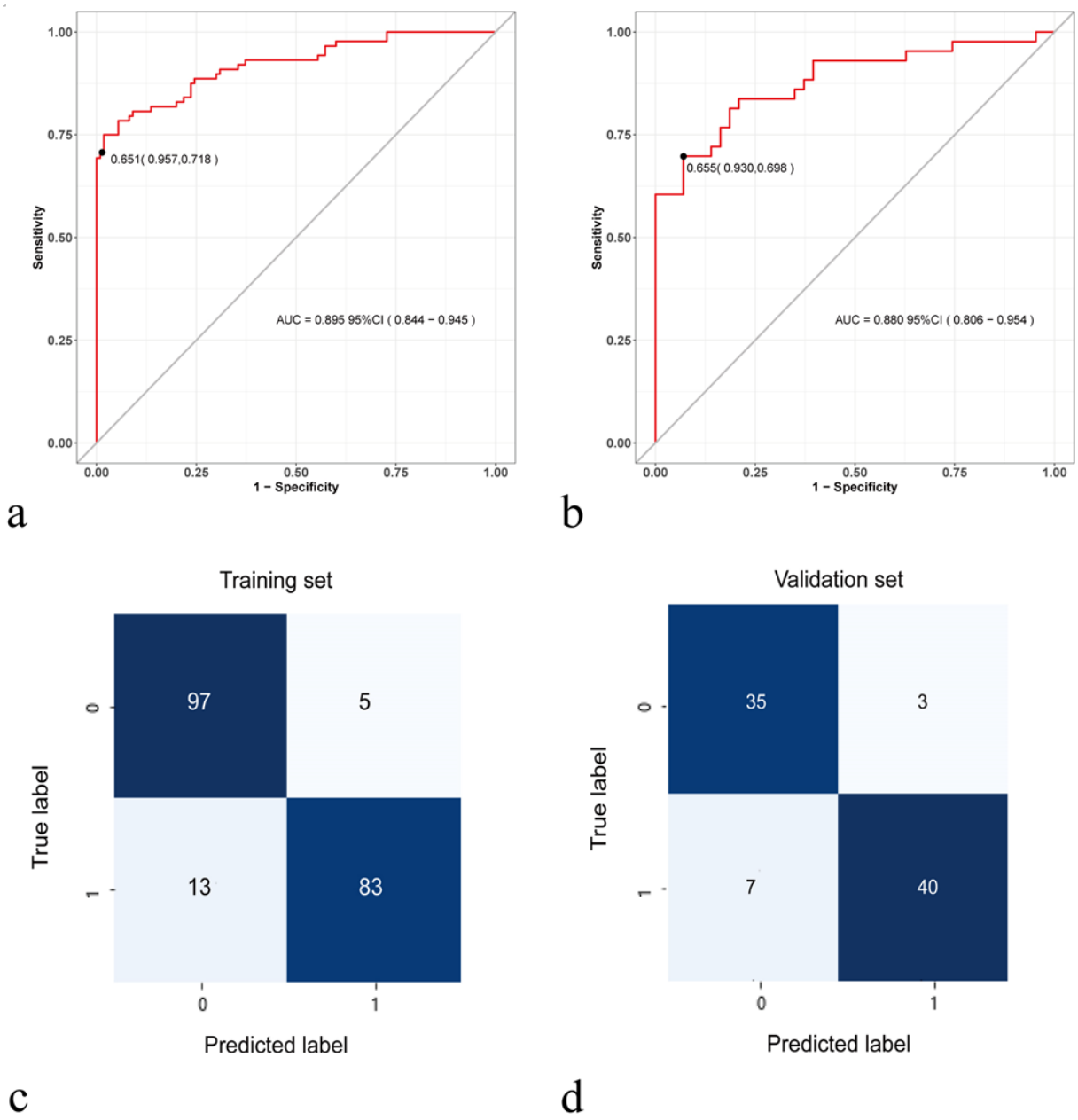

Figure 4. The ROC curve and confusion matrix for training set (a and c) and the validation set (b and d). ROC: receiver operator characteristic curve. AUC: area under the curve.

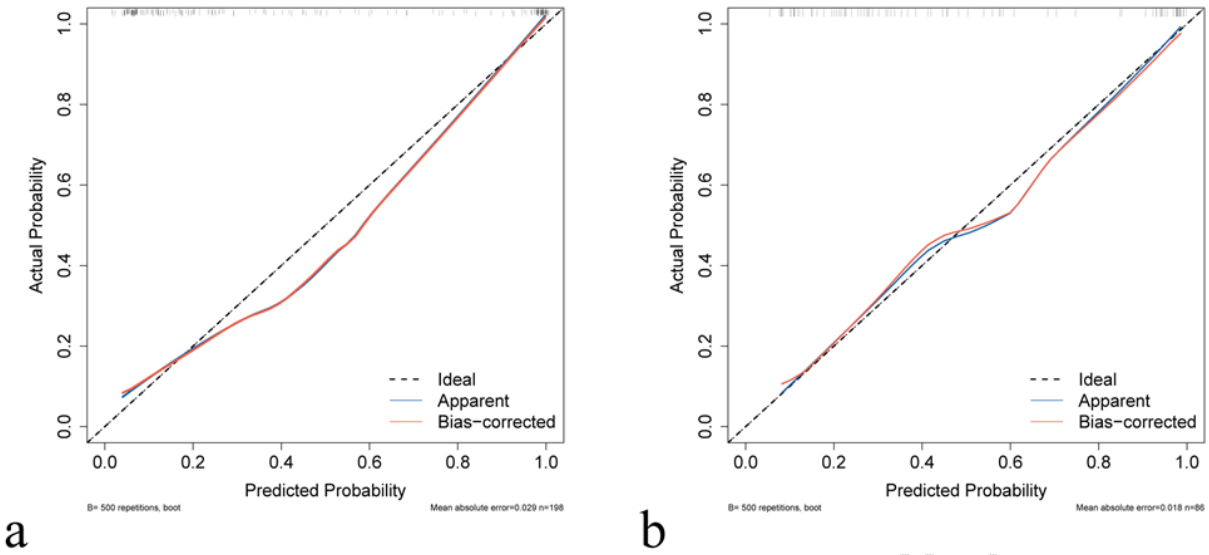

Figure 5. Nutritional risk prediction nomogram calibration curves. NRS2002 ⩾ 3 cases are depicted along the y-axis, and expected nutritional risks are displayed along the x-axis. A closer alignment with the diagonal dotted line, which represents an ideal model's flawless prediction, indicates a more precise forecast, as well as the solid line representing the performance of the training set (a) and validation set (b).

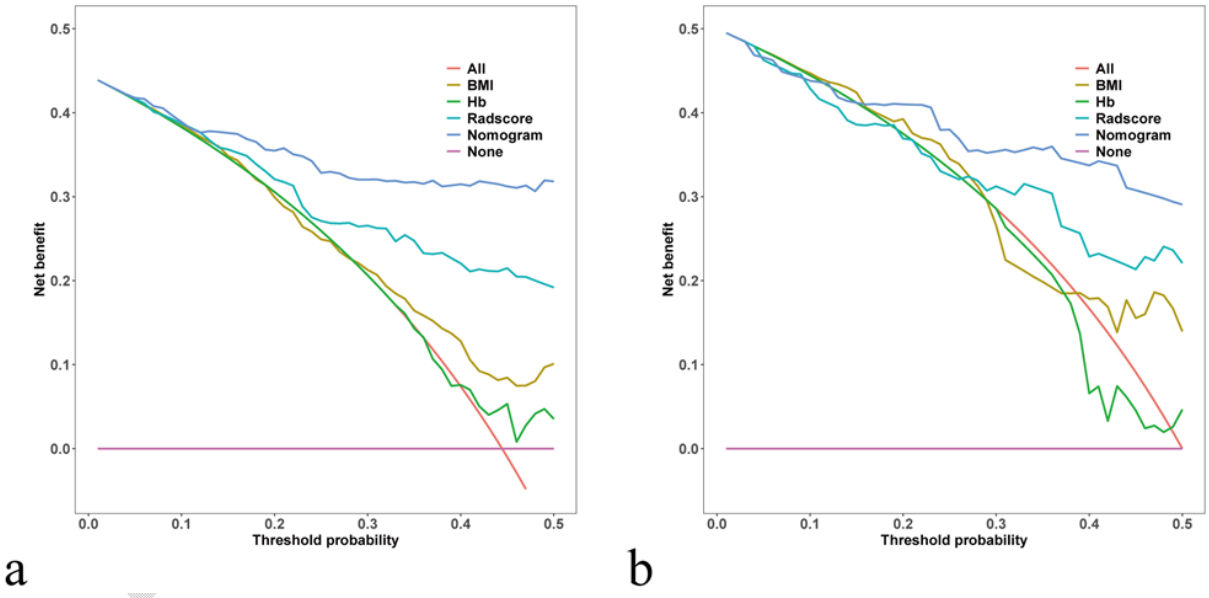

Figure 6. Nutritional risk nomogram decision curve analysis. The y-axis represents the net benefit. The blue solid line signifies the assumption that no patient is at nutritional risk, the red solid line indicates the assumption that every patient is at risk. Solid lines in other colours represents the risk nomogram. (a) from the training set. (b) from the validation set.

Supplementary Table 1. The list of radiomic features extracted from the VOIs

	Image type	Feature	Feature name
F1	original	shape	Elongation
F2		shape	MajorAxisLength
F3		shape	Maximum Diameter
F4		shape	MeshSurface
F5		shape	MinorAxisLength
F6		shape	Perimeter
F7		shape	PerimeterSurfaceRatio
F8		shape	PixelSurface
F9		shape	Sphericity
F10		firstorder	10Percentile
F11		firstorder	90Percentile
F12		firstorder	Energy
F13		firstorder	Entropy
F14		firstorder	Interquartile Range
F15		firstorder	Kurtosis
F16		firstorder	Maximum
F17		firstorder	MeanAbsoluteDeviation
F18		firstorder	Mean
F19		firstorder	Median
F20		firstorder	Minimum
F21		firstorder	Range
F22		firstorder	RobustMeanAbsoluteDeviation
F23		firstorder	RootMeanSquared
F24		firstorder	Skewness
F25		firstorder	TotalEnergy
F26		firstorder	Uniformity
F27		firstorder	Variance
F28		glcm	Autocorrelation
F29		glcm	ClusterProminence
F30		glcm	ClusterShade
F31		glcm	ClusterTendency
F32		glcm	Contrast
F33		glcm	Correlation
F34		glcm	DifferenceAverage
F35		glcm	DifferenceEntropy
F36		glcm	DifferenceVariance
F37		glcm	Id
F38		glcm	Idm
F39		glcm	Idmn
F40		glcm	Idn
F41		glcm	Imc1
F42		glcm	Imc2
F43		glcm	InverseVariance
F44		glcm	JointAverage
F45		glcm	JointEnergy
F46		glcm	JointEntropy
F47		glcm	MCC
F48		glcm	MaximumProbability
F49		glcm	SumAverage
F50		glcm	SumEntropy
F51		glcm	SumSquares
F52		gldm	DependenceEntropy
F53		gldm	DependenceNonUniformity
F54		gldm	DependenceNonUniformityNormalized
F55		gldm	Dependence Variance
F56		gldm	GrayLevelNonUniformity
F57		gldm	GrayLevelVariance
F58		gldm	HighGrayLevelEmphasis
F59		gldm	LargeDependenceEmphasis
F60		gldm	LargeDependenceHighGrayLevelEmphasis
F61		gldm	LargeDependenceLowGrayLevelEmphasis
F62		gldm	LowGrayLevelEmphasis
F63		gldm	SmallDependenceEmphasis
F64		gldm	SmallDependenceHighGrayLevelEmphasis
F65		gldm	SmallDependenceLowGrayLevelEmphasis

GLCM, gray-level co-occurrence matrix; GLRLM, gray-level run-length matrix; GLSZM, gray-level sizezone matrix; GLDM, gray-level dependence matrix; and NGTDM, neighboring gray-tone difference matrix

Supplementary Table 1. The list of radiomic features extracted from the VOIs (cont.)

	Image type	Feature	Feature name
F66	original	glrlm	GrayLevelNonUniformity
F67		glrlm	GrayLevelNonUniformityNormalized
F68		glrlm	GrayLevelVariance
F69		glrlm	HighGrayLevelRunEmphasis
F70		glrlm	LongRunEmphasis
F71		glrlm	LongRunHighGrayLevelEmphasis
F72		glrlm	LongRunLowGrayLevelEmphasis
F73		glrlm	LowGrayLevelRunEmphasis
F74		glrlm	RunEntropy
F75		glrlm	RunLengthNonUniformity
F76		glrlm	RunLengthNonUniformityNormalized
F77		glrlm	RunPercentage
F78		glrlm	RunVariance
F79		glrlm	ShortRunEmphasis
F80		glrlm	ShortRunHighGrayLevelEmphasis
F81		glrlm	ShortRunLowGrayLevelEmphasis
F82		glszm	GrayLevelNonUniformity
F83		glszm	GrayLevelNonUniformityNormalized
F84		glszm	GrayLevelVariance
F85		glszm	HighGrayLevelZoneEmphasis
F86		glszm	LargeAreaEmphasis
F87		glszm	LargeAreaHighGrayLevelEmphasis
F88		glszm	LargeAreaLowGrayLevelEmphasis
F89		glszm	LowGrayLevelZoneEmphasis
F90		glszm	SizeZoneNonUniformity
F91		glszm	SizeZoneNonUniformityNormalized
F92		glszm	SmallAreaEmphasis
F93		glszm	SmallAreaHighGrayLevelEmphasis
F94		glszm	SmallAreaLowGrayLevelEmphasis
F95		glszm	ZoneEntropy
F96		glszm	ZonePercentage
F97		glszm	ZoneVariance
F98		ngtdm	Busyness
F99		ngtdm	Coarseness
F100		ngtdm	Complexity
F101		ngtdm	Contrast
F102		ngtdm	Strength
F103	gradient	firstorder	10Percentile
F104		firstorder	90Percentile
F105		firstorder	Energy
F106		firstorder	Entropy
F107		firstorder	InterquartileRange
F108		firstorder	Kurtosis
F109		firstorder	Maximum
F110		firstorder	MeanAbsoluteDeviation
F111		firstorder	Mean
F112		firstorder	Median
F113		firstorder	Minimum
F114		firstorder	Range
F115		firstorder	RobustMeanAbsoluteDeviation
F116		firstorder	RootMeanSquared
F117		firstorder	Skewness
F118		firstorder	TotalEnergy
F119		firstorder	Uniformity
F120		firstorder	Variance
F121		glcm	Autocorrelation
F122		glcm	ClusterProminence
F123		glcm	ClusterShade
F124		glcm	ClusterTendency
F125		glcm	Contrast
F126		glcm	Correlation
F127		glcm	DifferenceAverage
F128		glcm	DifferenceEntropy
F129		glcm	DifferenceVariance
F130		glcm	Id

GLCM, gray-level co-occurrence matrix; GLRLM, gray-level run-length matrix; GLSZM, gray-level sizezone matrix; GLDM, gray-level dependence matrix; and NGTDM, neighboring gray-tone difference matrix

Supplementary Table 1. The list of radiomic features extracted from the VOIs (cont.)

	Image type	Feature	Feature name
F131	original	glcm	Idm
F132		glcm	Idmn
F133		glcm	Idn
F134		glcm	Imc1
F135		glcm	Imc2
F136		glcm	InverseVariance
F137		glcm	JointAverage
F138		glcm	JointEnergy
F139		glcm	JointEntropy
F140		glcm	MCC
F141		glcm	MaximumProbability
F142		glcm	SumAverage
F143		glcm	SumEntropy
F144		glcm	SumSquares
F145		gldm	DependenceEntropy
F146		gldm	DependenceNonUniformity
F147		gldm	DependenceNonUniformityNormalized
F148		gldm	Dependence Variance
F149		gldm	GrayLevelNonUniformity
F150		gldm	GrayLevelVariance
F151		gldm	HighGrayLevelEmphasis
F152		gldm	LargeDependenceEmphasis
F153		gldm	LargeDependenceHighGrayLevelEmphasis
F154		gldm	LargeDependenceLowGrayLevelEmphasis
F155		gldm	LowGrayLevelEmphasis
F156		gldm	SmallDependenceEmphasis
F157		gldm	SmallDependenceHighGrayLevelEmphasis
F158		gldm	SmallDependenceLowGrayLevelEmphasis
F159		glrlm	GrayLevelNonUniformity
F160		glrlm	GrayLevelNonUniformityNormalized
F161		glrlm	GrayLevelVariance
F162		glrlm	HighGrayLevelRunEmphasis
F163		glrlm	LongRunEmphasis
F164		glrlm	LongRunHighGrayLevelEmphasis
F165		glrlm	LongRunLowGrayLevelEmphasis
F166		glrlm	LowGrayLevelRunEmphasis
F167		glrlm	RunEntropy
F168		glrlm	RunLengthNonUniformity
F169		glrlm	RunLengthNonUniformityNormalized
F170		glrlm	RunPercentage
F171		glrlm	RunVariance
F172		glrlm	ShortRunEmphasis
F173		glrlm	ShortRunHighGrayLevelEmphasis
F174		glrlm	ShortRunLowGrayLevelEmphasis
F175		glszm	GrayLevelNonUniformity
F176		glszm	GrayLevelNonUniformityNormalized
F177		glszm	GrayLevelVariance
F178		glszm	HighGrayLevelZoneEmphasis
F179		glszm	LargeAreaEmphasis
F180		glszm	LargeAreaHighGrayLevelEmphasis
F181		glszm	LargeAreaLowGrayLevelEmphasis
F182		glszm	LowGrayLevelZoneEmphasis
F183		glszm	SizeZoneNonUniformity
F184		glszm	SizeZoneNonUniformityNormalized
F185		glszm	SmallAreaEmphasis
F186		glszm	SmallAreaHighGrayLevelEmphasis
F187		glszm	SmallAreaLowGrayLevelEmphasis
F188		glszm	ZoneEntropy
F189		glszm	ZonePercentage
F190		glszm	ZoneVariance
F191		glszm	Busyness
F192		glszm	Coarseness
F193		glszm	Complexity
F194		glszm	Contrast
F195		glszm	Strength

GLCM, gray-level co-occurrence matrix; GLRLM, gray-level run-length matrix; GLSZM, gray-level sizezone matrix; GLDM, gray-level dependence matrix; and NGTDM, neighboring gray-tone difference matrix

Supplementary Table 1. The list of radiomic features extracted from the VOIs (cont.)

	Image type	Feature	Feature name
F196	Lbp-2D	firstorder	10Percentile
F197		firstorder	90Percentile
F198		firstorder	Energy
F199		firstorder	Entropy
F200		firstorder	InterquartileRange
F201		firstorder	Kurtosis
F202		firstorder	Maximum
F203		firstorder	MeanAbsoluteDeviation
F204		firstorder	Mean
F205		firstorder	Median
F206		firstorder	Minimum
F207		firstorder	Range
F208		firstorder	RobustMeanAbsoluteDeviation
F209		firstorder	RootMeanSquared
F210		firstorder	Skewness
F211		firstorder	TotalEnergy
F212		firstorder	Uniformity
F213		firstorder	Variance
F214		glcm	Autocorrelation
F215		glcm	ClusterProminence
F216		glcm	ClusterShade
F217		glcm	ClusterTendency
F218		glcm	Contrast
F219		glcm	Correlation
F220		glcm	DifferenceAverage
F221		glcm	DifferenceEntropy
F222		glcm	DifferenceVariance
F223		glcm	Id
F224		glcm	Idm
F225		glcm	Idmn
F226		glcm	Idn
F227		glcm	Imc1
F228		glcm	Imc2
F229		glcm	InverseVariance
F230		glcm	JointAverage
F231		glcm	JointEnergy
F232		glcm	JointEntropy
F233		glcm	MCC
F234		glcm	MaximumProbability
F235		glcm	SumAverage
F236		glcm	SumEntropy
F237		glcm	SumSquares
F238		gldm	DependenceEntropy
F239		gldm	DependenceNonUniformity
F240		gldm	DependenceNonUniformityNormalized
F241		gldm	Dependence Variance
F242		gldm	GrayLevelNonUniformity
F243		gldm	GrayLevelVariance
F244		gldm	HighGrayLevelEmphasis
F245		gldm	LargeDependenceEmphasis
F246		gldm	LargeDependenceHighGrayLevelEmphasis
F247		gldm	LargeDependenceLowGrayLevelEmphasis
F248		gldm	LowGrayLevelEmphasis
F249		gldm	SmallDependenceEmphasis
F250		gldm	SmallDependenceHighGrayLevelEmphasis
F251		gldm	SmallDependenceLowGrayLevelEmphasis
F252		glrlm	GrayLevelNonUniformity
F253		glrlm	GrayLevelNonUniformityNormalized
F254		glrlm	GrayLevelVariance
F255		glrlm	HighGrayLevelRunEmphasis
F256		glrlm	LongRunEmphasis
F257		glrlm	LongRunHighGrayLevelEmphasis
F258		glrlm	LongRunLowGrayLevelEmphasis
F259		glrlm	LowGrayLevelRunEmphasis
F260		glrlm	RunEntropy

GLCM, gray-level co-occurrence matrix; GLRLM, gray-level run-length matrix; GLSZM, gray-level sizezone matrix; GLDM, gray-level dependence matrix; and NGTDM, neighboring gray-tone difference matrix

Supplementary Table 1. The list of radiomic features extracted from the VOIs (cont.)

	Image type	Feature	Feature name
F261		glrlm	RunLengthNonUniformity
F262		glrlm	RunLengthNonUniformityNormalized
F263		glrlm	RunPercentage
F264		glrlm	RunVariance
F265		glrlm	ShortRunEmphasis
F266		glrlm	ShortRunHighGrayLevelEmphasis
F267		glrlm	ShortRunLowGrayLevelEmphasis
F268		glszm	GrayLevelNonUniformity
F269		glszm	GrayLevelNonUniformityNormalized
F270		glszm	GrayLevelVariance
F271		glszm	HighGrayLevelZoneEmphasis
F272		glszm	LargeAreaEmphasis
F273		glszm	LargeAreaHighGrayLevelEmphasis
F274		glszm	LargeAreaLowGrayLevelEmphasis
F275		glszm	LowGrayLevelZoneEmphasis
F276		glszm	SizeZoneNonUniformity
F277		glszm	SizeZoneNonUniformityNormalized
F278		glszm	SmallAreaEmphasis
F279		glszm	SmallAreaHighGrayLevelEmphasis
F280		glszm	SmallAreaLowGrayLevelEmphasis
F281		glszm	ZoneEntropy
F282		glszm	ZonePercentage
F283		glszm	ZoneVariance
F284		ngtdm	Busyness
F285		ngtdm	Coarseness
F286		ngtdm	Complexity
F287		ngtdm	Contrast
F288		ngtdm	Strength
F289	Wavelet-LH	firstorder	10Percentile
F290		firstorder	90Percentile
F291		firstorder	Energy
F292		firstorder	Entropy
F293		firstorder	InterquartileRange
F294		firstorder	Kurtosis
F295		firstorder	Maximum
F296		firstorder	MeanAbsoluteDeviation
F297		firstorder	Mean
F298		firstorder	Median
F299		firstorder	Minimum
F300		firstorder	Range
F301		firstorder	RobustMeanAbsoluteDeviation
F302		firstorder	RootMeanSquared
F303		firstorder	Skewness
F304		firstorder	TotalEnergy
F305		firstorder	Uniformity
F306		firstorder	Variance
F307		glcm	Autocorrelation
F308		glcm	ClusterProminence
F309		glcm	ClusterShade
F310		glcm	ClusterTendency
F311		glcm	Contrast
F312		glcm	Correlation
F313		glcm	DifferenceAverage
F314		glcm	DifferenceEntropy
F315		glcm	DifferenceVariance
F316		glcm	Id
F317		glcm	Idm
F318		glcm	Idmn
F319		glcm	Idn
F320		glcm	Imc1
F321		glcm	Imc2
F322		glcm	InverseVariance
F323		glcm	JointAverage
F324		glcm	JointEnergy
F325		glcm	JointEntropy

GLCM, gray-level co-occurrence matrix; GLRLM, gray-level run-length matrix; GLSZM, gray-level sizezone matrix; GLDM, gray-level dependence matrix; and NGTDM, neighboring gray-tone difference matrix

Supplementary Table 1. The list of radiomic features extracted from the VOIs (cont.)

	Image type	Feature	Feature name
F326		glcm	MCC
F327		glcm	MaximumProbability
F328		glcm	SumAverage
F329		glcm	SumEntropy
F330		glcm	SumSquares
F331		gldm	DependenceEntropy
F332		gldm	DependenceNonUniformity
F333		gldm	DependenceNonUniformityNormalized
F334		gldm	Dependence Variance
F335		gldm	GrayLevelNonUniformity
F336		gldm	GrayLevelVariance
F337		gldm	HighGrayLevelEmphasis
F338		gldm	LargeDependenceEmphasis
F339		gldm	LargeDependenceHighGrayLevelEmphasis
F340		gldm	LargeDependenceLowGrayLevelEmphasis
F341		gldm	LowGrayLevelEmphasis
F342		gldm	SmallDependenceEmphasis
F343		gldm	SmallDependenceHighGrayLevelEmphasis
F344		gldm	SmallDependenceLowGrayLevelEmphasis
F345		glrlm	GrayLevelNonUniformity
F346		glrlm	GrayLevelNonUniformityNormalized
F347		glrlm	GrayLevelVariance
F348		glrlm	HighGrayLevelRunEmphasis
F349		glrlm	LongRunEmphasis
F350		glrlm	LongRunHighGrayLevelEmphasis
F351		glrlm	LongRunLowGrayLevelEmphasis
F352		glrlm	LowGrayLevelRunEmphasis
F353		glrlm	RunEntropy
F354		glrlm	RunLengthNonUniformity
F355		glrlm	RunLengthNonUniformityNormalized
F356		glrlm	RunPercentage
F357		glrlm	RunVariance
F358		glrlm	ShortRunEmphasis
F359		glrlm	ShortRunHighGrayLevelEmphasis
F360		glrlm	ShortRunLowGrayLevelEmphasis
F361		glszm	GrayLevelNonUniformity
F362		glszm	GrayLevelNonUniformityNormalized
F363		glszm	GrayLevelVariance
F364		glszm	HighGrayLevelZoneEmphasis
F365		glszm	LargeAreaEmphasis
F366		glszm	LargeAreaHighGrayLevelEmphasis
F367		glszm	LargeAreaLowGrayLevelEmphasis
F368		glszm	LowGrayLevelZoneEmphasis
F369		glszm	SizeZoneNonUniformity
F370		glszm	SizeZoneNonUniformityNormalized
F371		glszm	SmallAreaEmphasis
F372		glszm	SmallAreaHighGrayLevelEmphasis
F373		glszm	SmallAreaLowGrayLevelEmphasis
F374		glszm	ZoneEntropy
F375		glszm	ZonePercentage
F376		glszm	ZoneVariance
F377		ngtdm	Busyness
F378		ngtdm	Coarseness
F379		ngtdm	Complexity
F380		ngtdm	Contrast
F381		ngtdm	Strength
F382	wavelet-HL	firstorder	10Percentile
F383		firstorder	90Percentile
F384		firstorder	Energy
F385		firstorder	Entropy
F386		firstorder	InterquartileRange
F387		firstorder	Kurtosis
F388		firstorder	Maximum
F389		firstorder	MeanAbsoluteDeviation
F390		firstorder	Mean

GLCM, gray-level co-occurrence matrix; GLRLM, gray-level run-length matrix; GLSZM, gray-level sizezone matrix; GLDM, gray-level dependence matrix; and NGTDM, neighboring gray-tone difference matrix

Supplementary Table 1. The list of radiomic features extracted from the VOIs (cont.)

Image type	Feature	Feature name
F391	firstorder	Median
F392	firstorder	Minimum
F393	firstorder	Range
F394	firstorder	RobustMeanAbsoluteDeviation
F395	firstorder	RootMeanSquared
F396	firstorder	Skewness
F397	firstorder	TotalEnergy
F398	firstorder	Uniformity
F399	firstorder	Variance
F400	glcm	Autocorrelation
F401	glcm	ClusterProminence
F402	glcm	ClusterShade
F403	glcm	ClusterTendency
F404	glcm	Contrast
F405	glcm	Correlation
F406	glcm	DifferenceAverage
F407	glcm	DifferenceEntropy
F408	glcm	DifferenceVariance
F409	glcm	Id
F410	glcm	Idm
F411	glcm	Idmn
F412	glcm	Idn
F413	glcm	Imc1
F414	glcm	Imc2
F415	glcm	InverseVariance
F416	glcm	JointAverage
F417	glcm	JointEnergy
F418	glcm	JointEntropy
F419	glcm	MCC
F420	glcm	MaximumProbability
F421	glcm	SumAverage
F422	glcm	SumEntropy
F423	glcm	SumSquares
F424	gldm	DependenceEntropy
F425	gldm	DependenceNonUniformity
F426	gldm	DependenceNonUniformityNormalized
F427	gldm	Dependence Variance
F428	gldm	GrayLevelNonUniformity
F429	gldm	GrayLevelVariance
F430	gldm	HighGrayLevelEmphasis
F431	gldm	LargeDependenceEmphasis
F432	gldm	LargeDependenceHighGrayLevelEmphasis
F433	gldm	LargeDependenceLowGrayLevelEmphasis
F434	gldm	LowGrayLevelEmphasis
F435	gldm	SmallDependenceEmphasis
F436	gldm	SmallDependenceHighGrayLevelEmphasis
F437	gldm	SmallDependenceLowGrayLevelEmphasis
F438	glrlm	GrayLevelNonUniformity
F439	glrlm	GrayLevelNonUniformityNormalized
F440	glrlm	GrayLevelVariance
F441	glrlm	HighGrayLevelRunEmphasis
F442	glrlm	LongRunEmphasis
F443	glrlm	LongRunHighGrayLevelEmphasis
F444	glrlm	LongRunLowGrayLevelEmphasis
F445	glrlm	LowGrayLevelRunEmphasis
F446	glrlm	RunEntropy
F447	glrlm	RunLengthNonUniformity
F448	glrlm	RunLengthNonUniformityNormalized
F449	glrlm	RunPercentage
F450	glrlm	RunVariance
F451	glrlm	ShortRunEmphasis
F452	glrlm	ShortRunHighGrayLevelEmphasis
F453	glrlm	ShortRunLowGrayLevelEmphasis
F454	glszm	GrayLevelNonUniformity
F455	glszm	GrayLevelNonUniformityNormalized

GLCM, gray-level co-occurrence matrix; GLRLM, gray-level run-length matrix; GLSZM, gray-level sizezone matrix; GLDM, gray-level dependence matrix; and NGTDM, neighboring gray-tone difference matrix

Supplementary Table 1. The list of radiomic features extracted from the VOIs (cont.)

	Image type	Feature	Feature name
F456		glszm	GrayLevelVariance
F457		glszm	HighGrayLevelZoneEmphasis
F458		glszm	LargeAreaEmphasis
F459		glszm	LargeAreaHighGrayLevelEmphasis
F460		glszm	LargeAreaLowGrayLevelEmphasis
F461		glszm	LowGrayLevelZoneEmphasis
F462		glszm	SizeZoneNonUniformity
F463		glszm	SizeZoneNonUniformityNormalized
F464		glszm	SmallAreaEmphasis
F465		glszm	SmallAreaHighGrayLevelEmphasis
F466		glszm	SmallAreaLowGrayLevelEmphasis
F467		glszm	ZoneEntropy
F468		glszm	ZonePercentage
F469		glszm	ZoneVariance
F470		ngtdm	Busyness
F471		ngtdm	Coarseness
F472		ngtdm	Complexity
F473		ngtdm	Contrast
F474		ngtdm	Strength
F475	wavelength-HH	firstorder	10Percentile
F476		firstorder	90Percentile
F477		firstorder	Energy
F478		firstorder	Entropy
F479		firstorder	InterquartileRange
F480		firstorder	Kurtosis
F481		firstorder	Maximum
F482		firstorder	MeanAbsoluteDeviation
F483		firstorder	Mean
F484		firstorder	Median
F485		firstorder	Minimum
F486		firstorder	Range
F487		firstorder	RobustMeanAbsoluteDeviation
F488		firstorder	RootMeanSquared
F489		firstorder	Skewness
F490		firstorder	TotalEnergy
F491		firstorder	Uniformity
F492		firstorder	Variance
F493		glcm	Autocorrelation
F494		glcm	ClusterProminence
F495		glcm	ClusterShade
F496		glcm	ClusterTendency
F497		glcm	Contrast
F498		glcm	Correlation
F499		glcm	DifferenceAverage
F500		glcm	DifferenceEntropy
F501		glcm	DifferenceVariance
F502		glcm	Id
F503		glcm	Idm
F504		glcm	Idmn
F505		glcm	Idn
F506		glcm	Imc1
F507		glcm	Imc2
F508		glcm	InverseVariance
F509		glcm	JointAverage
F510		glcm	JointEnergy
F511		glcm	JointEntropy
F512		glcm	MCC
F513		glcm	MaximumProbability
F514		glcm	SumAverage
F515		glcm	SumEntropy
F516		glcm	SumSquares
F517		gldm	DependenceEntropy
F518		gldm	DependenceNonUniformity
F519		gldm	DependenceNonUniformityNormalized
F520		gldm	Dependence Variance

GLCM, gray-level co-occurrence matrix; GLRLM, gray-level run-length matrix; GLSZM, gray-level sizezone matrix; GLDM, gray-level dependence matrix; and NGTDM, neighboring gray-tone difference matrix

Supplementary Table 1. The list of radiomic features extracted from the VOIs (cont.)

	Image type	Feature	Feature name
F521		gldm	GrayLevelNonUniformity
F522		gldm	GrayLevelVariance
F523		gldm	HighGrayLevelEmphasis
F524		gldm	LargeDependenceEmphasis
F525		gldm	LargeDependenceHighGrayLevelEmphasis
F526		gldm	LargeDependenceLowGrayLevelEmphasis
F527		gldm	LowGrayLevelEmphasis
F528		gldm	SmallDependenceEmphasis
F529		gldm	SmallDependenceHighGrayLevelEmphasis
F530		gldm	SmallDependenceLowGrayLevelEmphasis
F531		glrlm	GrayLevelNonUniformity
F532		glrlm	GrayLevelNonUniformityNormalized
F533		glrlm	GrayLevelVariance
F534		glrlm	HighGrayLevelRunEmphasis
F535		glrlm	LongRunEmphasis
F536		glrlm	LongRunHighGrayLevelEmphasis
F537		glrlm	LongRunLowGrayLevelEmphasis
F538		glrlm	LowGrayLevelRunEmphasis
F539		glrlm	RunEntropy
F540		glrlm	RunLengthNonUniformity
F541		glrlm	RunLengthNonUniformityNormalized
F542		glrlm	RunPercentage
F543		glrlm	RunVariance
F544		glrlm	ShortRunEmphasis
F545		glrlm	ShortRunHighGrayLevelEmphasis
F546		glrlm	ShortRunLowGrayLevelEmphasis
F547		glszm	GrayLevelNonUniformity
F548		glszm	GrayLevelNonUniformityNormalized
F549		glszm	GrayLevelVariance
F550		glszm	HighGrayLevelZoneEmphasis
F551		glszm	LargeAreaEmphasis
F552		glszm	LargeAreaHighGrayLevelEmphasis
F553		glszm	LargeAreaLowGrayLevelEmphasis
F554		glszm	LowGrayLevelZoneEmphasis
F555		glszm	SizeZoneNonUniformity
F556		glszm	SizeZoneNonUniformityNormalized
F557		glszm	SmallAreaEmphasis
F558		glszm	SmallAreaHighGrayLevelEmphasis
F559		glszm	SmallAreaLowGrayLevelEmphasis
F560		glszm	ZoneEntropy
F561		glszm	ZonePercentage
F562		glszm	ZoneVariance
F563		ngtdm	Busyness
F564		ngtdm	Coarseness
F565		ngtdm	Complexity
F566		ngtdm	Contrast
F567		ngtdm	Strength
F568	wavelet-LL	firstorder	10Percentile
F569		firstorder	90Percentile
F570		firstorder	Energy
F571		firstorder	Entropy
F572		firstorder	InterquartileRange
F573		firstorder	Kurtosis
F574		firstorder	Maximum
F575		firstorder	MeanAbsoluteDeviation
F576		firstorder	Mean
F577		firstorder	Median
F578		firstorder	Minimum
F579		firstorder	Range
F580		firstorder	RobustMeanAbsoluteDeviation
F581		firstorder	RootMeanSquared
F582		firstorder	Skewness
F583		firstorder	TotalEnergy
F584		firstorder	Uniformity
F585		firstorder	Variance

GLCM, gray-level co-occurrence matrix; GLRLM, gray-level run-length matrix; GLSZM, gray-level sizezone matrix; GLDM, gray-level dependence matrix; and NGTDM, neighboring gray-tone difference matrix

Supplementary Table 1. The list of radiomic features extracted from the VOIs (cont.)

Image type	Feature	Feature name
F586	glcm	Autocorrelation
F587	glcm	ClusterProminence
F588	glcm	ClusterShade
F589	glcm	ClusterTendency
F590	glcm	Contrast
F591	glcm	Correlation
F592	glcm	DifferenceAverage
F593	glcm	DifferenceEntropy
F594	glcm	DifferenceVariance
F595	glcm	Id
F596	glcm	Idm
F597	glcm	Idmn
F598	glcm	Idn
F599	glcm	Imc1
F600	glcm	Imc2
F601	glcm	InverseVariance
F602	glcm	JointAverage
F603	glcm	JointEnergy
F604	glcm	JointEntropy
F605	glcm	MCC
F606	glcm	MaximumProbability
F607	glcm	SumAverage
F608	glcm	SumEntropy
F609	glcm	SumSquares
F610	gldm	DependenceEntropy
F611	gldm	DependenceNonUniformity
F612	gldm	DependenceNonUniformityNormalized
F613	gldm	Dependence Variance
F614	gldm	GrayLevelNonUniformity
F615	gldm	GrayLevelVariance
F616	gldm	HighGrayLevelEmphasis
F617	gldm	LargeDependenceEmphasis
F618	gldm	LargeDependenceHighGrayLevelEmphasis
F619	gldm	LargeDependenceLowGrayLevelEmphasis
F620	gldm	LowGrayLevelEmphasis
F621	gldm	SmallDependenceEmphasis
F622	gldm	SmallDependenceHighGrayLevelEmphasis
F623	gldm	SmallDependenceLowGrayLevelEmphasis
F624	glrlm	GrayLevelNonUniformity
F625	glrlm	GrayLevelNonUniformityNormalized
F626	glrlm	GrayLevelVariance
F627	glrlm	HighGrayLevelRunEmphasis
F628	glrlm	LongRunEmphasis
F629	glrlm	LongRunHighGrayLevelEmphasis
F630	glrlm	LongRunLowGrayLevelEmphasis
F631	glrlm	LowGrayLevelRunEmphasis
F632	glrlm	RunEntropy
F633	glrlm	RunLengthNonUniformity
F634	glrlm	RunLengthNonUniformityNormalized
F635	glrlm	RunPercentage
F636	glrlm	RunVariance
F637	glrlm	ShortRunEmphasis
F638	glrlm	ShortRunHighGrayLevelEmphasis
F639	glrlm	ShortRunLowGrayLevelEmphasis
F640	glszm	GrayLevelNonUniformity
F641	glszm	GrayLevelNonUniformityNormalized
F642	glszm	GrayLevelVariance
F643	glszm	HighGrayLevelZoneEmphasis
F644	glszm	LargeAreaEmphasis
F645	glszm	LargeAreaHighGrayLevelEmphasis
F646	glszm	LargeAreaLowGrayLevelEmphasis
F647	glszm	LowGrayLevelZoneEmphasis
F648	glszm	SizeZoneNonUniformity
F649	glszm	SizeZoneNonUniformityNormalized
F650	glszm	SmallAreaEmphasis

GLCM, gray-level co-occurrence matrix; GLRLM, gray-level run-length matrix; GLSZM, gray-level sizezone matrix; GLDM, gray-level dependence matrix; and NGTDM, neighboring gray-tone difference matrix

Supplementary Table 1. The list of radiomic features extracted from the VOIs (cont.)

Image type	Feature	Feature name
F651	glszm	SmallAreaHighGrayLevelEmphasis
F652	glszm	SmallAreaLowGrayLevelEmphasis
F653	glszm	ZoneEntropy
F654	glszm	ZonePercentage
F655	glszm	ZoneVariance
F656	ngtdm	Busyness
F657	ngtdm	Coarseness
F658	ngtdm	Complexity
F659	ngtdm	Contrast
F660	ngtdm	Strength

GLCM, gray-level co-occurrence matrix; GLRLM, gray-level run-length matrix; GLSZM, gray-level sizezone matrix; GLDM, gray-level dependence matrix; and NGTDM, neighboring gray-tone difference matrix

Supplementary Table 2. The radiomics features selected by LASSO regression analysis

Radiomics features	Coefficients
gradient_glcm_lmc2	0.04341
gradient_glrlm_LowGrayLevelRunEmphasis	0.01522
gradient_glszm_SmallAreaLowGrayLevelEmphasis	0.03121
gradient_ngtdm_Coarseness	0.024431
wavelet-LH_gldm_SmallDependenceLowGrayLevelEmphasis	0.019694
wavelet-LL_glszm_SmallAreaLowGrayLevelEmphasis	0.005178

GLCM, gray-level co-occurrence matrix; GLRLM, gray-level run-length matrix; GLSZM, gray-level sizezone matrix; GLDM, gray-level dependence matrix; and NGTDM, neighboring gray-tone difference matrix

Supplementary Table 3. Characteristics of 284 gastric cancer patients enrolled in the study according to the NRS2002 score

	All patients N=284	Training set N=198	Validation set N=86	p-value
Gender, n (%)				0.137
Male	181 (63.73%)	91 (59.48%)	90 (68.70%)	
Female	103 (36.27%)	62 (40.52%)	41 (31.30%)	
Age(years)	56.00 [46.00;63.25]	55.00 [46.00;62.00]	57.00 [46.50;65.00]	0.145
BMI (kg/m^2)	19.46 [17.74;21.51]	19.77 [18.83;22.98]	18.65 [16.64;20.07]	<0.001
Diabetic, n (%)				0.540
No	272 (95.77%)	145 (94.77%)	127 (96.95%)	
Yes	12 (4.23%)	8 (5.23%)	4 (3.05%)	
Smoking, n (%)				0.860
No	186 (65.49%)	99 (64.71%)	87 (66.41%)	
Yes	98 (34.51%)	54 (35.29%)	44 (33.59%)	
Hb(g/L)	115.90 [99.45;131.05]	126.00 [114.00;139.30]	103.00 [87.95;115.90]	<0.001
NEUT(109/L)	3.54 [2.70;4.22]	3.56 [2.81;4.19]	3.42 [2.52;4.34]	0.519
TLC(109/L)	1.75 [1.38;2.21]	1.91 [1.47;2.29]	1.68 [1.26;1.94]	<0.001
ALB(g/L)	39.25 [36.70;41.20]	39.80 [37.70;41.50]	37.80 [34.45;40.70]	<0.001
PAB(g/L)	212.55 [180.40;256.82]	206.90 [180.50;250.60]	217.00 [179.70;270.00]	0.370
TC(mmol/L)	4.62 [4.05;5.14]	4.77 [4.24;5.18]	4.52 [3.88;5.02]	0.004
AFP(ng/mL)	7.87 [5.58;11.60]	7.84 [5.50;11.78]	7.90 [5.60;11.10]	0.907
CEA(ng/mL)	2.51 [1.85;3.52]	2.75 [1.89;3.46]	2.41 [1.71;3.52]	0.179
CA125(U/mL)	10.55 [7.58;14.64]	10.17 [7.30;13.42]	11.63 [8.00;17.80]	0.010
CA153(U/mL)	7.87 [5.58;11.60]	7.84 [5.50;11.78]	7.90 [5.60;11.10]	0.916
CA199(U/mL)	7.68 [4.18;17.31]	6.93 [4.23;16.58]	9.20 [3.63;18.60]	0.626
T stage				0.667
T0	2 (0.70%)	2 (1.31%)	0 (0.00%)	
T1	59 (20.77%)	32 (20.92%)	27 (20.61%)	
T2	44 (15.49%)	23 (15.03%)	21 (16.03%)	
T3	43 (15.14%)	20 (13.07%)	23 (17.56%)	
T4	136 (47.89%)	76 (49.67%)	60 (45.80%)	
N stage				0.372
N0	108 (38.03%)	60 (39.22%)	48 (36.64%)	
N1	40 (14.08%)	17 (11.11%)	23 (17.56%)	
N2	53 (18.66%)	32 (20.92%)	21 (16.03%)	
N3	83 (29.23%)	44 (28.76%)	39 (29.77%)	
Radscore	7.73 [5.82;14.35]	6.06 [4.87;7.42]	15.07 [9.36;16.83]	<0.001

BMI, body mass index; HB, hemoglobin; ALB, albumin; PAB, prealbumin; NEUT, neutrophile count; TLC, total lymphocyte count; CEA, carcinoembryonic antigen; AFP, alpha-fetoprotein.
p<0.05 meant that the difference was statistically significant.

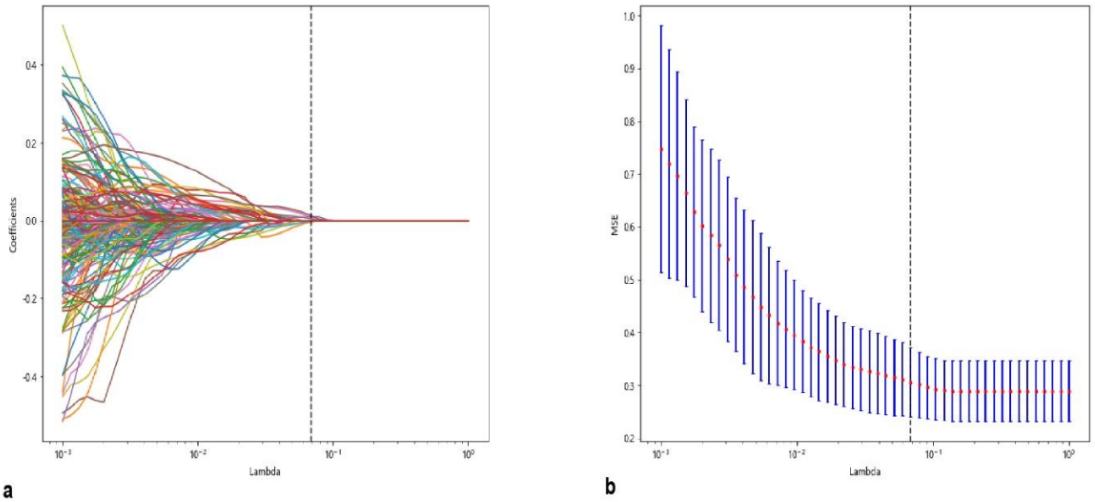

Supplementary Figure 1. Radiomic features selection using the LASSO logistic regression model. (a) LASSO coefficient profiles of the 102 radiomics features. The coefficients (y-axis) were plotted against the log (lambda), and the radiomics signature was constructed utilizing the selected 6 radiomic features with non-zero coefficients. (b) Plotting the partial likelihood deviance against log (lambda). The lower x-axis indicate the log (lambda). The y-axis denotes the partial likelihood of deviance. Utilizing the minimum criteria, vertical lines (dotted) were created at the optimal values. The minimum criteria-based 10-fold cross-validation was utilized for the selection of the tuning parameter (λ) in the LASSO model.

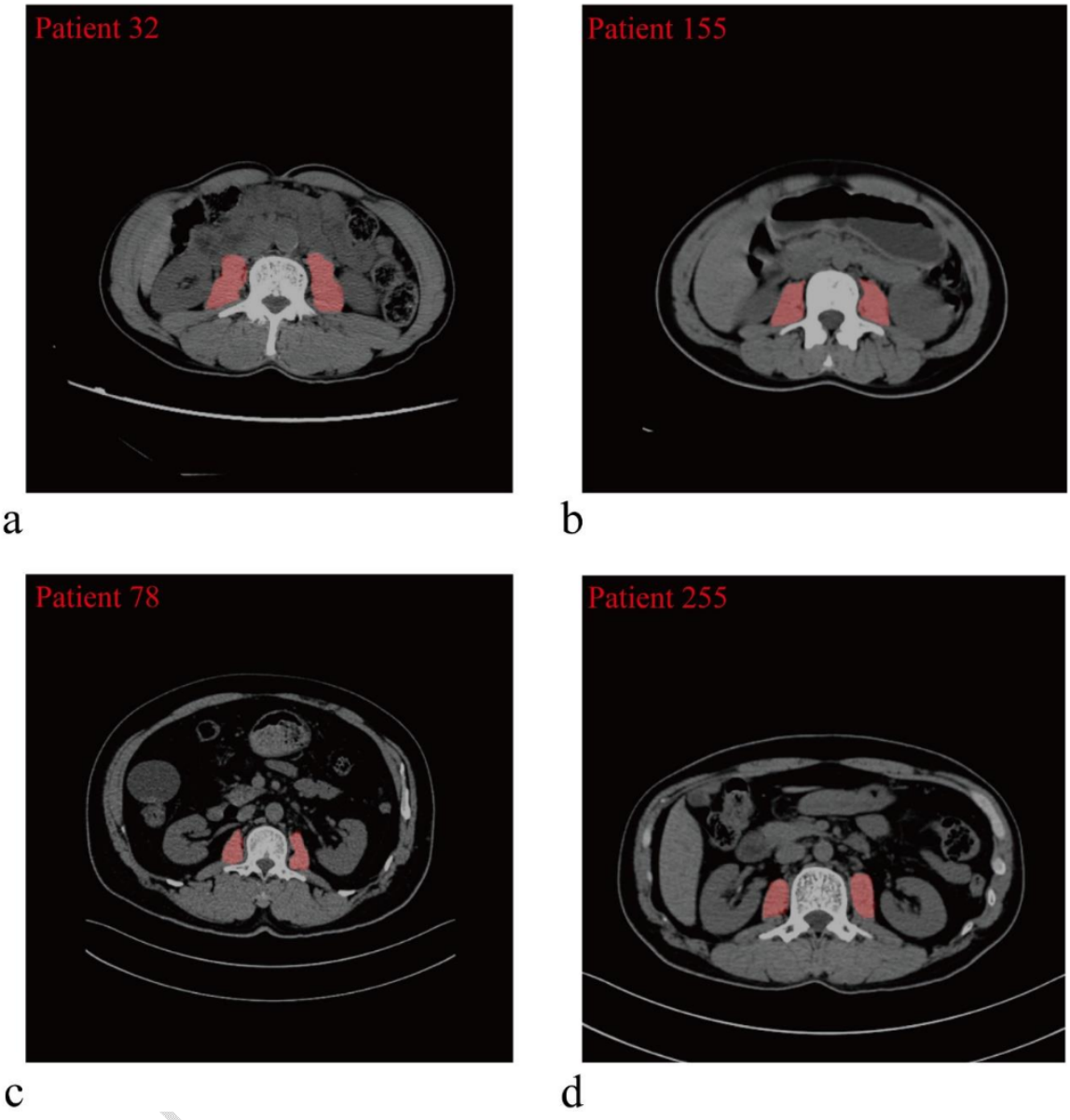

Supplementary Figure 2. Abdominal computed tomography images of the third lumbar vertebra level in four patients with gastric cancer. Patients with NRS2002 scores <3 (a and b). Patients with NRS2002 scores ≥3 (c and d)

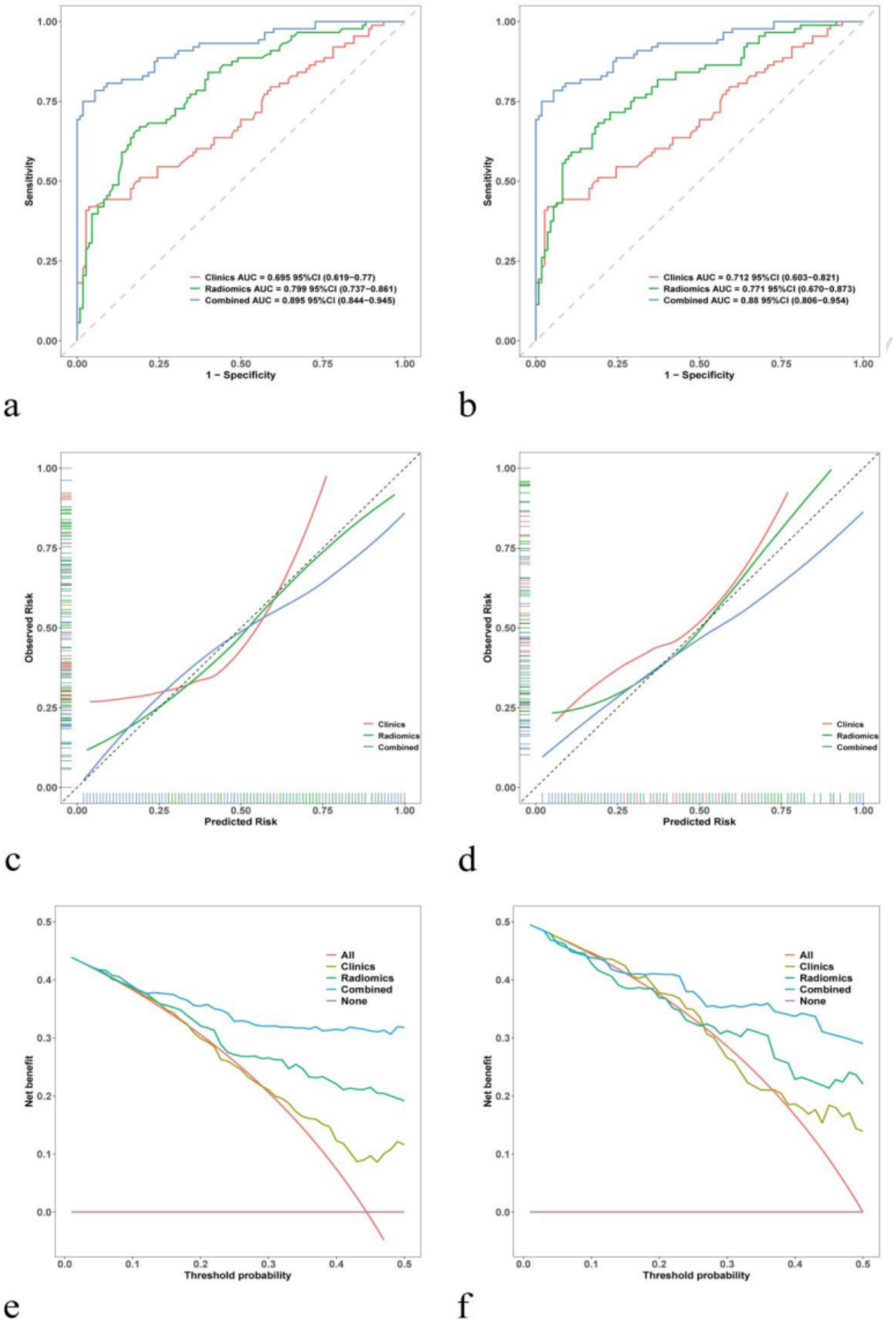

Supplementary Figure 3. Validation and comparison of clinical, radiomics and combined models. The receiver operator characteristic curve for training set (a) and the validation set (b). The calibration curves for training set (c) and the validation set (d). The decision curve analysis for training set (c) and the validation set (f).